Astron. Astrophys. 360, 213–226 (2000)

ASTRONOMY AND ASTROPHYSICS

The composition of the circumstellar dust around the Herbig Ae stars AB Aur and HD 163296

J. Bouwman[1], **A. de Koter**[1], **M.E. van den Ancker**[1,3], **and L.B.F.M. Waters**[1,2]

[1] Astronomical Institute "Anton Pannekoek", University of Amsterdam, Kruislaan 403, 1098 SJ Amsterdam, The Netherlands
[2] Instituut voor Sterrenkunde, K.U. Leuven, Celestijnenlaan 200 B, 3001 Heverlee, België
[3] Harvard-Smithsonian Center for Astrophysics, 60 Garden Street, MS 42, Cambridge, MA 02138, USA

Received 20 January 2000 / Accepted 10 May 2000

Abstract. We have analysed the 2–200 μm ISO spectra of two bright Herbig Ae stars, AB Aur and HD 163296, in order to derive the composition and mass over temperature distribution of the circumstellar dust. We find that the two stars have a similar composition of the dust, however also with some important differences. We address the onset of the strong near-infrared emission between 1–4 μm. We show that this emission can be explained with thermal emission from metallic iron or dust species containing iron. The circumstellar dust surrounding both stars shows two distinct regimes in the mass over temperature distributions with temperatures of $\sim 10^3$ and $\sim 10^2$ K. Modelling of the ISO spectra further reveal a significant deviation of the derived grain sizes compared to the interstellar grain size distribution. A population of large ($\sim$ 1 mm) grains is required to explain the observed (sub-) millimetre fluxes of HD 163296. The presence of crystalline silicates and the larger grain sizes in HD 163296 compared to AB Aur suggests that the former star is a more evolved system. Amorphous silicates make out the bulk of the dust mass in both stars. It is likely that a significant fraction of the dust is carbon-rich. We find strong evidence for a 20–30 μm band which we tentatively attribute to FeO.

Key words: radiative transfer – stars: circumstellar matter – stars: formation – stars: individual: AB Aur – stars: individual: HD 163296 – stars: pre-main sequence

1. Introduction

HAEBE stars represent the final stage of pre-main-sequence (PMS) evolution of intermediate-mass stars ($\sim$ 2–10 $M_\odot$). As a consequence of the star formation process these stars are typically surrounded by a gas and dust envelope and/or disk. They may be the precursors of young main sequence β-Pictoris and Vega-type stars. These latter systems are surrounded by circumstellar debris disks, which perhaps contain planetary bodies. This would imply that the environment around HAEBE stars represents an early phase in the formation of planets. ISO spectroscopy of isolated HAEBE stars has strengthened this link between HAEBE stars and planet formation. Malfait et al. (1998b) showed that the ISO spectrum of the B9Ve star HD 100546 has a high abundance of crystalline silicates, and that the composition of the dust in this object is remarkably similar to that seen in the solar system comet Hale-Bopp (Crovisier et al. 1997). Moreover, the Fe star HD 142527 shows evidence for hydro-silicates, indicative of aquateous alteration of silicates in its cold circumstellar disk (Malfait et al. 1999), which is expected only to occur on the surfaces of larger bodies.

This paper is the second in a series in which we will study the circumstellar environment around the Herbig Ae/Be (HAEBE) stars AB Aurigae (A0Ve+sh) and HD 163296 (A1Ve). We have choosen to investigate these two stars because *(i)* their basic properties are well known, *(ii)* they are isolated and bright, making them ideal candidates to study their circumstellar material, *(iii)* they are nearby systems that have been spatially resolved in CO; HD 163296 has also been resolved in the continuum at 1.3 mm, and *(iv)* on the whole the two stars are very similar. The last point implies that differences in spectral energy distribution may be linked to differences in dust composition and morphology. This can provide important insights in the evolution of the circumstellar dust and may yield information on characteristic time scales of dust evolution (from comparison with stellar age) and/or on the importance of properties of the natal molecular cloud, such as initial cloud size, mass and angular momentum.

In the first paper (van den Ancker et al. 2000, hereafter Paper I) we presented new infrared spectra of these two well studied stars obtained with the Short- and Long Wavelength Spectrometers on board the *Infrared Space Observatory* (ISO) (Kessler et al. 1996). In this paper we present quantitative spectroscopic modelling with the aim to constrain dust properties such as composition, abundance and size- and shape-distribution. In a subsequent paper we intend to present a detailed multi-dimensional model for the dust distribution around these HAEBE systems.

The geometry of the circumstellar environment around HAEBE stars remains a persistent problem. The key issue is that the observational evidence from spectral energy distributions (SEDs) and spectroscopy do not define the geometry of the circumstellar dust in a unique way (see Waters & Waelkens 1998 for a review). We will start out by summarizing this evidence immediately focusing on AB Aur and HD 163296. The second

Send offprint requests to: J. Bouwman (jeroenb@astro.uva.nl)

Table 1. Astrophysical parameters of the programme stars

	AB Aur	Ref.	HD 163296	Ref.
α (2000)	04 55 45.79	(1)	17 56 21.26	(1)
δ (2000)	+30 33 05.5	(1)	$-$21 57 19.5	(1)
d [pc]	144^{+23}_{-17}	(2)	122^{+17}_{-13}	(2)
Sp. Type	A0Ve+sh	(3)	A1Ve	(8)
V [m]	7.03–7.09†	(4)	6.82–6.89	(4)
A_V [m]	0.50$\pm$0.06	(5)	0.31$\pm$0.06	(5)
$T_{\rm eff}$ [K]	9520^{+500}_{-300}	(5)	9230^{+300}_{-500}	(5)
$\log g$	4.07	(5)	4.10	(5)
$L_\star$ [L$_\odot$]	47$\pm$12	(2)	32$\pm$8	(2)
$R_\star$ [R$_\odot$]	2.5$\pm$0.5	(5)	2.2$\pm$0.5	(5)
$M_\star$ [M$_\odot$]	2.4$\pm$0.2	(2)	2.3$\pm$0.1	(2)
log(Age) [yr]	6.3$\pm$0.2	(2)	6.6$\pm$0.4	(2)
$v \sin i$ [km s^{-1}]	80$\pm$5	(6)	120$\pm$1	(9)
CO disk size [AU^2]	405 $\times$ 100‡	(7)	310 $\times$ 160	(7)
i [$^\circ$]	76	(7)	58	(7)
P.A. [$^\circ$]	$+79^{+2}_{-3}$	(7)	$+126^{+2}_{-3}$	(7)

† *Note:* Older photographic measurements (Gaposchkin et al. 1952) show values up to $m_{pg} = 8.4$.
‡ Corrected for revised distance (van den Ancker et al. 1997).

References: (1) Hipparcos Catalogue; (2) van den Ancker et al. (1997); (3) Böhm & Catala (1993); (4) van den Ancker et al. (1998); (5) Paper I, but relevant parameters have been scaled such that they are conform spectral type A1Ve and not A3Ve; (6) Böhm & Catala (1995); (7) Mannings & Sargent (1997); (8) Houk & Smith-Moore (1988); (9) Halbedel (1996).

important problem addressed in this paper is the nature of the onset of near-IR emission. This will be discussed in Sect. 1.2.

1.1. Geometry of the circumstellar dust

In view of the similarity to their less massive counterparts the T Tauri stars, HAEBE stars are expected to have optically thick disks. Indeed, in the case of AB Aur high-resolution imaging together with a de-convolution method (Marsh et al. 1995), indicates a disk of size 36 and 72 AU at 11.7 and 17.9 μm respectively, adopting a distance of 144 pc. Direct observational evidence for a disk-like geometry comes from the kinematical properties of ^{13}CO gas, observed in the $J = 1 \rightarrow 0$ pure rotational transition in AB Aur and CO gas, observed in the $J = 2 \rightarrow 1$ pure rotational transition in HD 163296 which seem consistent with a rotating Keplerian disk (Mannings & Sargent 1997, Mannings et al. 1997). The dimension of the CO emitting regimes has been estimated to be $\sim 405 \times 100$ AU, and $\sim 310 \times 160$ AU for AB Aur and HD 163296 respectively. The aspect ratio's imply that we see AB Aur almost edge-on at an inclination angle of 76° and HD 163296 at 58°. For this last star the continuum emission at 1.3 mm has been spatially resolved, showing an elongated structure with dimension $\sim 110 \times 95$ AU. Near-infrared interferometric observations of AB Aur (Millan-Gabet et al. 1999) have resolved the inner part of the dust distribution, determining the inner edge of the dust to be at 0.3 AU (see also Sect. 1.2). An upper limit on the inclination in this inner regime is determined to be 45°, suggesting that the inner and outer regions of the disk do not have the same geometry.

The shape of the IR spectral energy distribution has often been used as a diagnostic for constraining the geometry of the HAEBE surroundings. In some cases, the SED may provide firm constraints especially when a lack in balance is found between energy absorbed in the UV and optical and energy re-emitted in the IR (Meeus et al. 1998). Such a discrepancy strongly points to a disk-like structure. One should, however, be very careful with conclusions relating to the spatial distribution of the dust derived from the SED only (e.g. Henning et al. 1998, Bouwman et al. 1999).

Evidence for the presence of a large optically thin medium comes from the strong 9.7 μm silicate *emission* (Cohen 1980, Sitko 1981, van den Ancker et al. 2000) observed in both stars. If the silicates are located in a geometrically thin disk, modelling shows one expects this disk to be optically thick at optical as well as IR wavelengths. However, it is substantially more difficult (if not impossible) to reconcile the presence of this emission adopting an optically thick "disk-only" model compared to assuming an optically thin emitting region. So, if a disk is expected on the basis of imaging, the silicate emission at least suggests the presence of an optically thin region of substantial size above the surface of this disk (e.g Chiang & Goldreich 1997). The forbidden [O I] λ 6300 emission (Corcoran & Ray 1997), which is narrow (± 30 kms^{-1}), symmetric and unshifted in AB Aur, could be formed in such an extended surface layer or disk atmosphere, and be broadened by Keplerian rotation.

The above arguments imply that the geometry of the CSM around these stars is likely to be complex, i.e. it cannot be explained by a "disk-only" model. Most likely only the inner part of the disk is optically thick and a substantial thin region, such as an extended surface layer or (flared) outer disk region – or both – is present as well.

1.2. The onset of near-IR emission

An important aspect of the geometry of the CSM of HAEBE stars is the innermost region where the hottest dust grains are present and which dominate the near-IR SED. The key question here is whether one is able to understand the onset of near-IR emission (from ~ 2 μm) in terms of a physically realistic scenario. The remarkable uniformity of the onset of near-IR emission in HAEBE systems (Meeus et al. in prep.) suggests a similar geometry and/or dust grain population at high (~ 1500 K) temperatures at the inner regions of the CSM. In the following we will discuss several possible explanations for the near-IR onset.

Hillenbrand et al. (1992) suggested a model in which the observed near-IR flux is due to accretion luminosity from a geometrically thin active accretion disk. The emission in the NIR is explained in this model with (high temperature) accreting gas in the innermost part of the disk. Emission at longer wavelengths would be due to dust in an optically thick disk. The accretion

Table 2. Sources of the optical constants

Species	Solid State	Wavelength [μm]	T_{cond} [K]	Ref.
$[Mg,Fe]_2SiO_4$	A	0.2–500	1400	(1)
FeO	C	0.2–500	1000	(2)
C	G	0.01–1000	1000	(3)
C	A	0.1–800	1000	(4)
H_2O	A (ice)	0.05–1000	150	(5)
Mg_2SiO_4	C	0.04–3.4	1400	(6)
		4–250		(7)
Fe	M	0.1–10^5	1500	(8)
FeS	C	0.1–10^5	720	(8)

Abbreviations used to designate the solid state: A = Amorphous; C = Crystalline; G = Grafitic; M = Metallic.

References: (1) Dorschner et al. (1995); (2) Henning et al. (1995); (3) Laor & Drain (1993); (4) Preibisch et al. (1993); (5) Warren (1984); (6) Scott & Duley (1996); (7) Servoin & Piriou (1973); (8) Henning & Stognienko (1996).

rates Hillenbrand et al. (1992) derive are $1.5 \cdot 10^{-6}$ and $1.3 \cdot 10^{-6}$ $M_\odot yr^{-1}$ for AB Aur and HD 163296 respectively. Radio continuum observations (Skinner et al. 1993) point to much smaller accretion rates of $1.1 \cdot 10^{-8}$ and $\leq 9.1 \cdot 10^{-9}$ $M_\odot yr^{-1}$ for AB Aur and HD 163296 respectively, which are inconsistent with the high accretion rates needed in the Hillenbrand model. Also the lack of substantial veiling at optical wavelengths points towards small accretion rates. Böhm & Catala (1993) derived an upper limit for the accretion rate of AB Aur, from the veiling of photospheric lines, of $< 7.5 \cdot 10^{-8}$ $M_\odot yr^{-1}$, consistent with Skinner et al. (1993). The strongest objection against the active accretion disk model comes from interferometric observations of AB Aur (Millan-Gabet et al. 1999) which can not be reproduced using this model.

A different explanation for the near-IR emission could be Polycyclic Aromatic Hydrocarbons (PAHs), of which the emission bands are located at 3.4, 6.2, 7.7, 8.6 and 11.3 μm. This makes PAHs a candidate for explaining the near-IR flux. Due to their small size, the characteristic temperature of PAH particles can be high as they are no longer expected to be in thermodynamic equilibrium. Quantum heating effects result in such high temperatures that their dominant emission is in the near-IR. To account for all observed near-IR emission however very high abundances are required (Natta et al. 1993) which seem unlikely. Even though their narrow characteristic features are present in AB Aur, it is not expected that PAHs are also responsible for the broad continuum contribution starting at ~ 2 μm. This conclusion is strengthened by the shape and strength of the near-IR emission in HD 163296, which is identical to AB Aur but shows no PAH bands (van den Ancker et al. 2000). A different explanation seems required.

One of the main points of this paper is that observed near-IR emission in the programme stars can be explained simply by dust in thermodynamic equilibrium. The dust species that have strong resonances in this spectral region ($\sim$ 1–8 μm) are metallic iron, iron oxide, and carbonaceous dust grains, either graphitic or 'amorphous'. The dust grains are heated by stellar radiation in the inner parts of the circumstellar disk up to the dust destruction temperatures of the individual dust species. We will show that in view of the high grain temperatures (~ 1500 K) needed to produce the observed flux at near-IR wavelengths, metallic iron grains are the most likely candidates to explain the onset of the near-IR emission (see Sect. 3.1). With our model we can also reproduce the interferometric observations by Millan-Gabet et al. (1999) of AB Aur, showing an inner hole of 0.3 AU.

This paper is organized as follows: in Sect. 2 we discuss the chosen approach to model the ISO spectra and describes the model we used. Sect. 3 gives the results of the model fitting and a discussion over the implications of these results is presented in Sect. 4. We summarize our results in Sect. 5.

2. Method and assumptions

2.1. Model approach and assumptions

In this study we have chosen to model the CSM of the programme stars using a simple optically thin dust model. In view of the above discussion it is clear that this is a simplified approach. Still, we have adopted this approach for the following reasons:

(i) A main focus of this paper is to identify and model the solid-state features present in the rich ISO spectra of AB Aur and HD 163296. For this, we employ a library of laboratory measurements of the optical constants of approximately fifty different grain materials of interest. From this collection we selected eight species, listed in Table 2, which are most likely present in Herbig Ae/Be systems. These species are discussed in the next subsection. We attempt to constrain composition, abundances, size distributions, shape properties and mass over temperature distribution of the dust grains present. This goal requires an extended parameter study, which at the present day cannot be done using a consistent multi-dimensional dust transfer model.

(ii) The above discussion on the geometry of the CSM around AB Aur and HD 163296 shows that part of the emission originates from an extended optically thin medium, e.g. the broad emission complex from $\sim$ 14 to 28 μm and the 9.7 μm silicate emission, and which suggests that the optically thin model has at least partial validity.

Still, the next step should be to model these two nearby Herbig Ae systems using a 2D-model. Any constraints on the chemical properties derived in this exploratory study will then contribute significantly to the feasibility of such a complex follow-up investigation. Below, we will discuss model assumptions and adopted optical properties of the dust constituents.

In order to model IR spectra we have developed the radiative transfer code MODUST. This code treats the transfer of radiation through spherical density distributions of dust grains. The (multiple) dust shells are irradiated by a central source, either a black body or a Kurucz model. Any prescription for the dust distribution in the shell may be adopted. In the present analysis, we use this model in the optically thin mode so as to

be able to perform an extensive parameter study. In the models used to fit the spectra of AB Aur and HD 163296 we assumed a power law shape for the density $\rho(r)$ as well as for the grain size distribution $n(a)$, i.e.

$$\rho(r) = \rho_0 \left(\frac{r}{R_{\rm in}}\right)^{-p} \quad \text{and,} \tag{1}$$

$$n(a) = A \left(\frac{a}{a_{\rm min}}\right)^{-m} \tag{2}$$

The shell is confined between an inner and outer edge. ρ_0 is the density at the inner edge $R_{\rm in}$ of the dust shell. Grain sizes range between a minimum $a_{\rm min}$ and maximum size. The constant A in the equation for the grain size distribution is a normalization constant depending on the bulk density and size distribution of the grains. A power-law gives a good description of a grain size distribution. Observations of interstellar extinction show a size distribution with $m = 3.5$ (Mathis et al., 1977). Theoretical work (Biermann & Hartwit 1980) predicts a power-law distribution whenever there is shattering and coagulation of grains through grain-grain collisions. Dust condensation models (e.g Dominik et al. 1989) also predict a power law distribution to be applicable over a large range of grain sizes. We use a multi-component mixture of grain species where the grains are homogeneous in composition and in bulk density. Table 2 lists the grain species of interest we used for our modelling (for a discussion see below). We used the optical constants from laboratory measurements to calculate the extinction properties; for a discussion we refer to the references given in Table 2. At present our model incorporates spherical dust grains, for which we use Mie calculations, and a continuous distribution of ellipsoidal dust grains, for which we use CDE calculations to determine the absorption and scattering coefficients (see Bohren & Huffman 1983 for a full review on these methods). Table 2 also lists the wavelength ranges in which laboratory measurements were available. Outside these ranges we made the following extrapolations. At short wavelengths, i.e. in the UV or optical, the dielectric function $\epsilon = \epsilon' + i\epsilon''$ can be extrapolated by,

$$\epsilon' \simeq 1 - \frac{\omega_{\rm p}^2}{\omega^2} \tag{3}$$

$$\epsilon'' \simeq \frac{\gamma\omega_{\rm p}^2}{\omega^3} \tag{4}$$

With ω the frequency, $\omega_{\rm p}$ the plasma frequency, and γ a damping factor of the electromagnetic wave. Both insulators and metals show the same behaviour at these wavelengths. These extrapolations are reasonable for wavelengths shorter than $\approx 0.2\,\mu$m. At long wavelengths (sub-millimetre and millimetre) there is a marked difference in optical properties between grains of different solid-state structure, composition and shape. In this regime, we therefore extrapolate the extinction coefficient,

$$C_{\rm ext} \approx \frac{1}{\lambda^\alpha} \tag{5}$$

with α equal to 1 for amorphous and CDE dust grains and $\alpha = 2$ for spherical metallic and crystalline grains.

The temperature distribution of the dust follows from the equation of radiative equilibrium. The adopted optically thin limit implies that the dust particles absorb the full radiation from the direction of the stellar disk only. One can easily show that if the absorption coefficient of the dust would behave as a power law, $Q_{\rm abs} \propto \nu^p$, then the resulting temperature structure at sufficient distance from the star is also given by a power law, with slope $T(r) \propto r^{-2/(p+4)}$. Although in reality $Q_{\rm abs}$ contains resonances, the overal run of temperature is usually well represented by a power law. Therefore, in the remainder of this paper, we will characterize the temperature distribution by providing the values at the minimum and maximum radius only.

2.2. Adopted chemical composition of the dust

From the SWS and LWS spectra one can derive information about the mass over temperature distribution of the dust, and by looking at spectral features, about the chemical composition of the dust. However, if only spectral information is available the geometry and properties of the circumstellar material can not be uniquely determined (e.g Bouwman et al. 1999). To determine such properties as density and grain size distribution one has to constrain the models either by supplementary observations, such as imaging, or by using theoretical arguments, e.g concerning dust destruction temperatures, crystallisation time-scales or grain removal by radiation pressure.

One of the main difficulties with the determination of the chemical composition of the circumstellar dust by comparison with laboratory measurements, is that solid-state resonance bands are rather broad. With different grain species contributing at the same wavelengths, this will result in a more or less continuous spectra without a clear spectral signature that can be uniquely attributed to a single grain species. Exceptions to this are for instance the crystalline silicates such as forsterite (Mg_2SiO_4) and enstatite ($MgSiO_3$) which have strong and narrow resonances in the IR, and the vibrational modes in disordered (amorphous) silicate grains around $10\,\mu$m. To determine which dust species contribute at parts of the spectra where no clear spectral feature is present, additional constraints need to be imposed (e.g. abundance constraints, condensation temperature of the individual dust species). Taking the results of dust nucleation models, one can estimate which dust species are present.

We assume that all the Mg, Fe, and Si is incorporated into dust grains. Evidence for this comes from abundance studies of the ISM, which show a correlation between heavy element depletion and density in the ISM (O'Donnel & Mathis 1997). This points to a very efficient mechanism for accretion of these species in dust grains. Studies of these elements in the gas phase also show abundances less than solar. This could be a result of either very hardy dust grains or could indicate that the elements in the ISM have abundances less than solar. The observed near solar gas-phase abundance of S points to a solar composition of the ISM (Fitzpatrick & Spitzer 1997), suggesting Mg, Fe and Si are in grains which are very difficult to destroy. If so, the ratio of iron plus magnesium to silicon atoms in the dust (3.4:1) is

Table 3. Model fit parameters of AB Aur and HD 163296. Listed are the parameters defining the density and grain size distribution, the chemical composition and the mass fraction $\mathrm{M_{frac}}$ of the individual dust species in both the hot as well as the cold dust component. Note that the given value for $\rho_0 = \rho(R_{\rm in})$, i.e. the density at the inner radius of the shell, assumes that all dust species exist at $R_{\rm in}$ irrespective of the condensation temperature. In reality, we only have a dust species present if its temperature is below $\mathrm{T_{cond}}$ (see Table 2). This implies that for the hot component, the density at the inner radius is slightly modified, i.e. it is somewhat lower.

	HD 163296		AB Aur	
Component:	Hot	Cold	Hot	Cold
Radius	1–10 AU	30–511 AU	1–11 AU	28–175 AU
$\rho(r)$	$\propto r^{-1}$	$\propto r^{-1}$	$\propto r^{-1}$	$\propto r^{-1}$
ρ_0 [gr cm^{-3}]	$1.5 \cdot 10^{-18}$	$2.4 \cdot 10^{-16}$	$1.3 \cdot 10^{-18}$	$4.0 \cdot 10^{-16}$
$\mathrm{M_{dust}/M_\odot}$	$2.9 \cdot 10^{-9}$	$2.0 \cdot 10^{-4}$	$2.6 \cdot 10^{-9}$	$3.3 \cdot 10^{-5}$
T range	1500–200 K	300–20 K	1500–200 K	400–50 K
n(a)	$\propto a^{-2.4}$	$\propto a^{-2.0}$	$\propto a^{-2.8}$	$\propto a^{-2.0}$
Dust species:				
	$\mathrm{M_{frac}}$ a [μm]	$\mathrm{M_{frac}}$ a [μm]	$\mathrm{M_{frac}}$ a [μm]	$\mathrm{M_{frac}}$ a [μm]
Olivine	0.73 0.01–6.0	0.76 0.1–1260	0.71 0.01–5.0	0.74 0.01–126
Carbon	0.13 0.01–2.0	0.17 0.1–200	0.16 0.01–2.0	0.11 0.01–32.0
Water Ice	– –	0.07 0.1–25.0	– –	0.15 0.1–40.0
Iron	0.03 0.01–0.08	– –	0.06 0.01–0.1	– –
Iron Oxide	0.04 –	$3 \cdot 10^{-5}$ –	0.07 –	$9 \cdot 10^{-4}$ –
Forsterite	0.07 0.01–2.0	$2 \cdot 10^{-3}$ 0.1–5.0	– –	– –

greater than the maximum ratio that can be accounted for by silicate grains alone (2:1). This result seems to imply that a substantial fraction of the iron or magnesium is in a grain population other than silicates (Fitzpatrick 1997). Theoretical work on dust condensation (Gail & Sedlmayer 1999) shows that metallic iron could be one of the primary condensates in outflows around M-type giants. Most of the Mg will be incorporated into silicate. Iron can enter the silicate at a lower temperature forming iron rich amorphous silicates (Gail 1998). In the ISM, metallic iron can be oxidized to FeO at temperatures below 400 K on a time scales $t_{\rm ox} \geq (a/10{\rm nm})10^8/n_{\rm H}{\rm yr}$ (Jones 1990). Taking a typical density of $n_{\rm H} \sim 100$ cm^{-3} in diffuse clouds, small iron grains (0.01–0.1 μm) will be fully oxidized in 10^6–10^7 year. In view of typical lifetimes of diffuse clouds (10^7–10^8 yr), one may expect that all small Fe grains are oxidized. This also seems to be confirmed by mass spectrometer data on Halley and chemical analysis of interplanetary dust particles (IDPs) (Bradley et al. 1992; Schulze et al. 1997). These studies show that most Mg is confined to silicates but that Fe is also incorporated in different materials such as metals, oxides and sulphides.

The nature of the carbonaceous dust is not clear. The only direct observational evidence for the presence of carbon around the Herbig Ae stars comes from the observed PAH features around AB Aur and from the presence of carbon ions in their winds and in in-falling gas. The carbonaceous dust in the ISM is modelled with a variety of materials (for a overview see Henning 1997). Most models include graphite and a form of disordered carbon. Since one is looking at (reprocessed) interstellar dust one can expect these materials also to be present around young stellar objects (YSOs).

3. Results

In this section we present the results for the composition and abundance study of the grain population in AB Aur and HD 163296. We have split this presentation in a discussion of the near IR properties on the one hand, and of the far IR properties on the other hand. However, we start out with a discussion of those properties that we found to be similar for both stars.

In Fig. 1 we present the SWS & LWS spectra together with ground-based and IRAS photometry (see Paper I). Overplotted in these figures are the current best model fits. The parameters of these model fits are listed in Table 3. The most striking feature in these spectra appear to be the presence of two distinct dust components, a relatively hot dust component with a mass averaged temperature of $\sim$1000 K and a relatively cold dust component with a mass averaged temperature of $\sim$100 K. This bi-modal temperature structure in the circumstellar dust surrounding both Herbig Ae stars is best seen in the spectrum of HD 163296, where for wavelengths shorter than 40 μm the hot dust component dominates the spectrum, while for longer wavelengths the Wien tail of the cold dust component starts to dominate the SED. In a similar way the cold dust in AB Aur starts to dominate the spectrum longward of 30 μm. The total dust mass derived from the model fits in the cold dust component is $\sim 3 \cdot 10^{-5}$ and $\sim 2 \cdot 10^{-4}$ $\mathrm{M_\odot}$ for AB Aur and HD 163296 respectively. The mass ratio of the hot over the cold dust component is $\sim 10^{-4}$–10^{-5}, so by far most of the mass is contained in the cold component. In view of the uncertainties in the modelling discussed in the next sections the derived masses are uncertain by a factor of two to three. A blow-up covering the ISO SWS and LWS wavelength region for both stars is shown

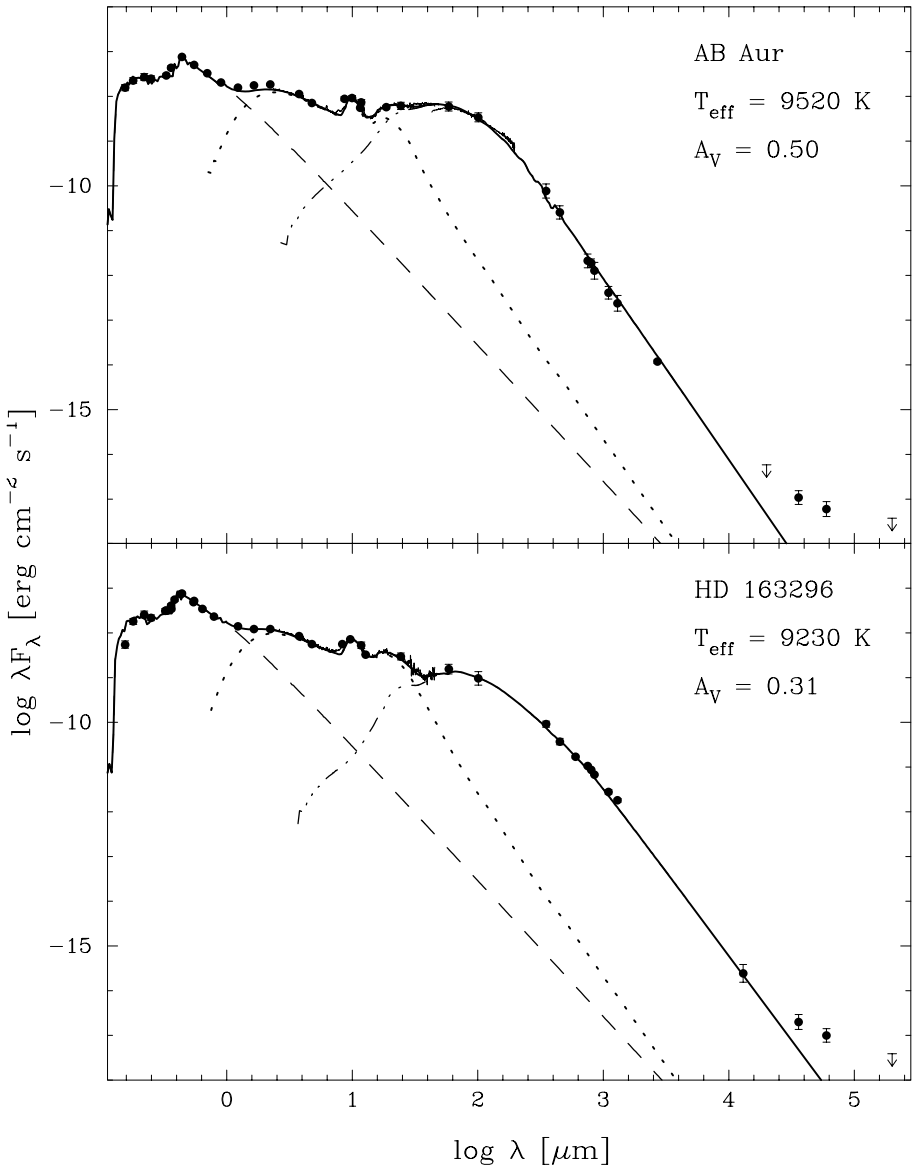

Fig. 1. Model fit to the spectral energy distribution (SED) of AB Aur (top) and HD 163296 (bottom). The solid dots indicate ground-based and IRAS photometry corrected for extinction. Also plotted are the ISO-SWS spectra, and for AB Aur the ISO-LWS spectrum. The dashed lines represent Kurucz models for the stellar photospheres. The dotted lines show the contribution from the hot dust component and the dot-dashed lines the contribution from the cold dust component. Indicated in the figure are the effective temperature of the adopted Kurucz model and the line-of-sight visual extinction at maximum brightness.

in Fig. 2. Again we include the best model fits but now we have indicated the relative contribution of all individual dust species.

The features in the observed spectra of AB Aur and HD 163296 have been described in detail in Paper I. Therefore we only briefly discuss the most prominent ones relevant for the model fitting. Both stars show a rather flat continuum up to $\sim$ 8 μm, similar to the observed near-IR fluxes of other HAEBE stars. A prominent broad amorphous silicate band is present around $\sim$ 10 μm due to the Si-O stretching mode. HD 163296 clearly shows the presence of a broad emission complex between $\sim$ 20–35 μm in which olivine bending modes have an important contribution. In AB Aur this complex does not appear as pronounced, because the cool component already starts to dominate the spectrum longwards of $\sim 30\,\mu$m. The main difference in spectral signature between the stars is that AB Aur shows emission bands at 6,2, 7.7, 8.6 and 11.2 μm, usually ascribed to polycyclic aromatic hydrocarbons (PAH) while HD 163296 does not show these bands. Conversely, the spectrum of HD 163296 reveals crystalline silicates at 11.3, 16.3, 17.8, 23.5, 31.3 and 33.5 μm, while AB Aur does not appear to have any crystalline material.

3.1. The 2–8 μm spectral region

We first concentrate on modelling the flat near-IR continuum from 2–8 μm. The presented results are essentially equally valid for both AB Aur and HD 163296. We identified several dust species that can reproduce the observed continuum flux. These are metallic iron, iron oxide and a carbonaceous dust component, either graphite or a more "amorphous" form of carbon dust. Due to the lack of clear spectral signatures in this wavelength region, the possibility of confusion of the relative contribution of individual dust species exists.

As an example Fig. 3 shows three different models for the near-IR flux of AB Aur which are spectroscopically indistinguishable from one another. The chemical composition of the

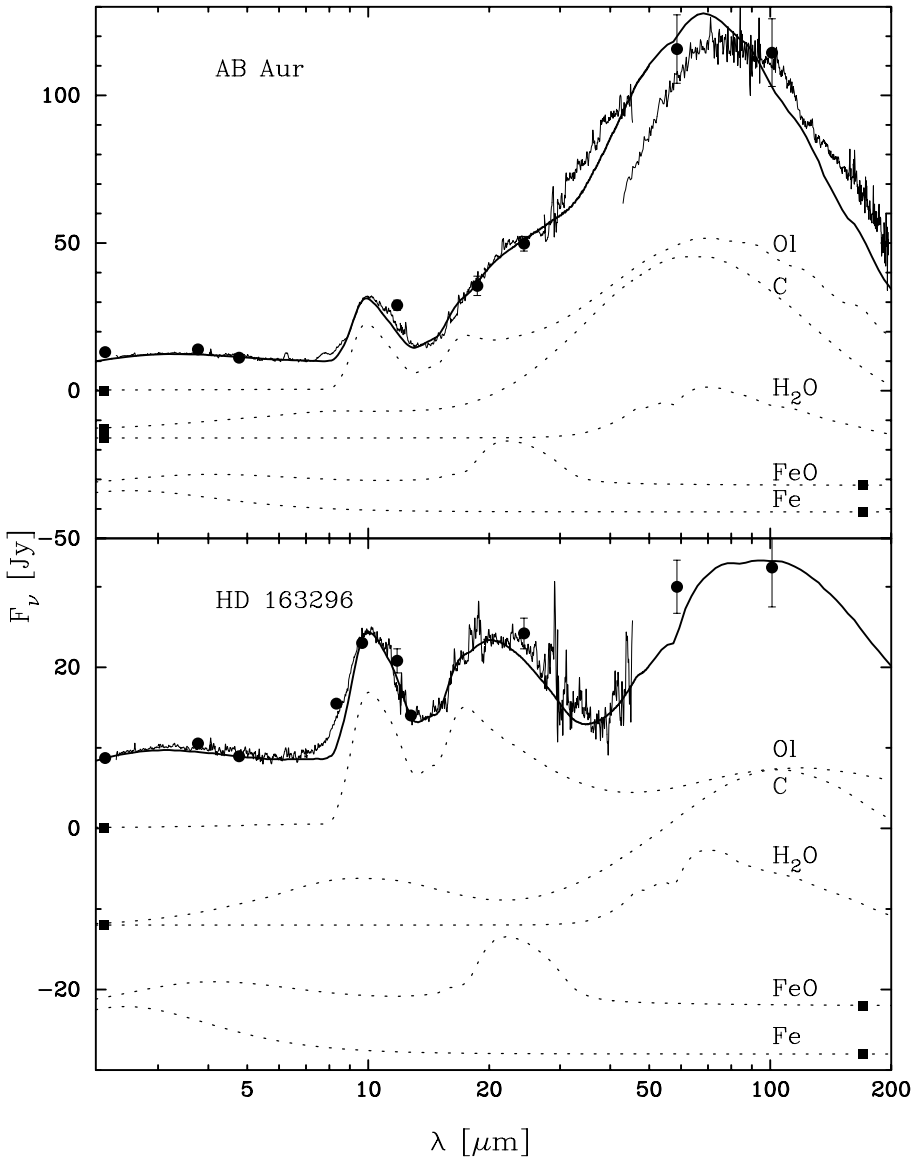

Fig. 2. Model fit to the ISO spectra of AB Aur and HD 163296. The solid dots indicate ground based and IRAS photometry. The dotted lines represent the contributions to the continuum flux of the individual dust components. The curves are offset for clarity. The squares indicate the zero flux level for each component.

three solutions is given in the figure caption. It is clear, one has to introduce secondary arguments to distinguish between these models. The highest grain temperature required to reproduce the observed flux at the shortest wavelengths is ∼1500 K, which exceeds the grain evaporation temperature of iron oxide, but is at the condensation temperature of metallic iron and carbonaceous grains (e.g. Gail 1998). However, at about ∼1000 K, carbon grains become subject to chemical sputtering (oxidation) and will be destroyed before reaching the condensation temperature (Duschl et al. 1996; Finocchi et al. 1997). This also applies to amorphous carbon grains (AMC), which cannot reproduce the observed flux between 2 and 4 μm even when heated up to 1500 K. The only dust species that can reproduce the observed flux at these short wavelengths with an acquired grain temperature up to 1500 K is metallic iron. A satisfactory fit to this part of the spectrum could only be achieved when the temperature distribution of the iron grains ranged between ∼ 700–1500 K. When more grains at lower temperature where included, we were not able to reproduce the flat near-IR spectrum. The continuum longwards of 4 μm can be reproduced by thermal emission of iron oxide and carbonaceous grains heated to their grain destruction temperatures. Iron oxide however does not easily reach temperatures close to its condensation temperature as above ∼ 400 K it is slowly converted into solid iron (H.-P. Gail priv. comm.). In Fig. 2 we have indicated the contribution of each individual dust species to the total flux. This clearly shows that metallic iron is the chemical species responsible for the 2–4 μm fluxes. For the dust at $T < 1000$ K we have used amorphous carbon in our model fits, however graphite cannot be ruled out on spectroscopic grounds.

For the model fit to AB Aur, additional constraints on the dust properties near the inner boundary can be obtained using recent interferometric observations (Millan-Gabet et al. 1999). Fig. 4 shows the visibility curves of three models to the NIR spectrum of the star. These visibilities essentially probe the innermost region of the disk, where the emission is dominated by

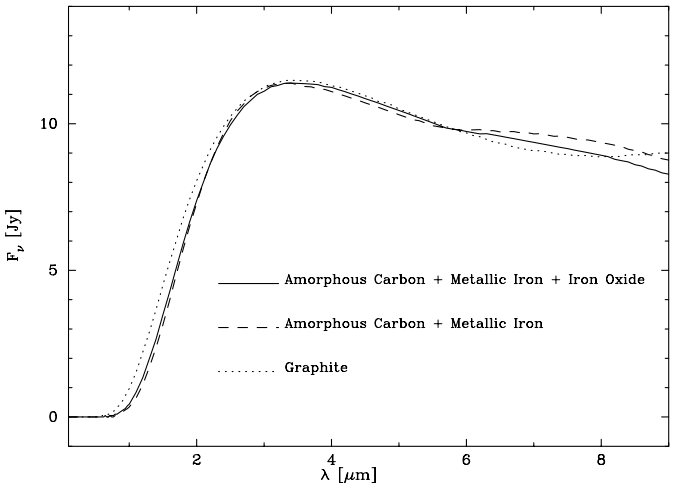

Fig. 3. Continuum dust emission from dust species contributing to the NIR between 2 and 8 μm for three different models. The solid line indicates a model consisting of amorphous carbon, metallic iron and iron oxide, with mass fractions of 0.55, 0.2 and 0.25 respectively. The dashed line indicates a model with only amorphous carbon and metallic iron with mass fractions of 0.53 and 0.47 respectively. The dotted line indicates a model where the entire NIR emission is due to graphite.

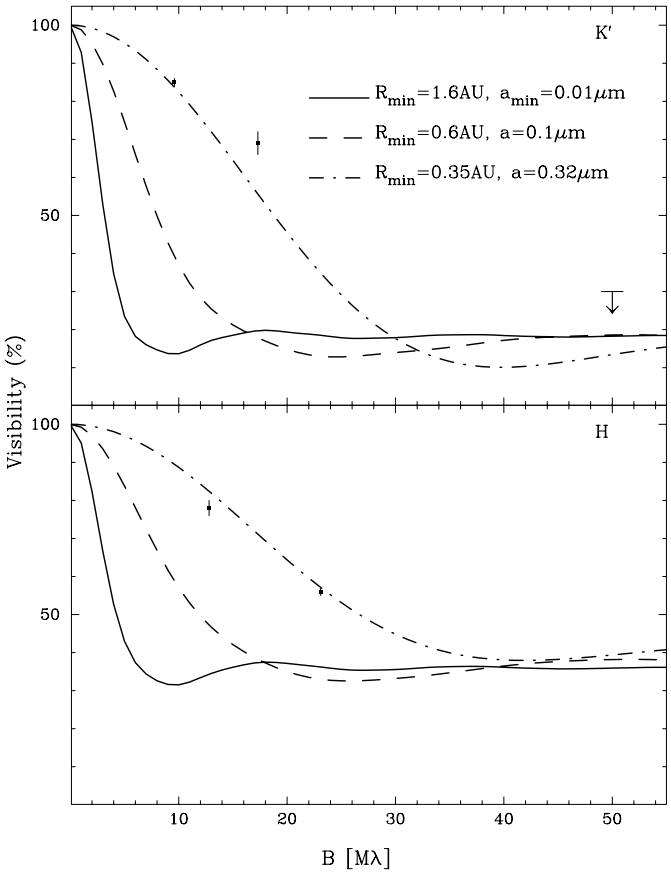

Fig. 4. Visibility curves of three model fits of the metallic iron component to the NIR spectrum of AB Aur as a function of baseline length. The black squares indicate the observational data with the error bars indicating the rms error. The top panel shows the visibility in the K–band, and the bottom panel the H-band. The solid line indicates the current best fit, while the dashed and dot-dashed line indicate models with a single grain size of 0.1 and 0.32 μm respectively.

the metallic iron grains. The solid line gives the best fit model, in which Fe grains in sizes from 0.01 to 0.1 μm are used. Note that this model does *not* reproduce the observed visibilities in the K- and H-band. Also shown in the figure are the resulting visibility curves using models containing only single sized Fe grains of 0.1 and 0.32 μm, respectively. Note that both these models yield identical fits to the observed spectrum as does the best fit model. The 0.32 μm grain model fits the visibility best. The associated inner radius of the iron dust at 0.35 AU is consistent with that found by Millan-Gabet et al. (1999). This result is therefore suggestive that grain evaporation plays an important rôle in the inner part of the proto-planetary disk, where only the largest grains, having the lowest temperature, survive to a distance of $\sim$ 0.3 AU of the central star. However, the latter model would lead to a discontinuity in the spatial distribution with respect to the other dust species. This is because our current models do not consistently incorporate the destruction of dust grains.

3.2. The 8–30 μm region

Substantial contribution to the flux around 10 μm in both Herbig Ae stars comes from disordered (amorphous) silicates (see Fig. 2). The width of the silicate feature is such that it cannot be fitted with a single-size dust distribution, which would yield an emission feature which is too narrow. A size distribution is required in which the smallest grains contribute most to the short wavelength side of the 10 μm silicate feature, while the largest grains contribute to the long wavelength tail. Though a clear spectral signature for the silicates exists and confusion with emission from other species is not a problem, a different type of degeneracy exists in the modelling. For a fixed grain composition the shape and strength of the SEDs is determined by the mass over temperature distribution and the emissivity of the dust. Fig. 5a shows three model fits for the silicate emission around AB Aur for different grain size distributions all having the same mass over temperature distribution. The value given in Table 3 (and represented by the solid line in Fig. 5a) for the power of the grain size distribution is the mean value between the limiting cases (dashed and dashed-dotted lines) for which a model fit could be made. Though an uncertainty in the exact grain size distribution remains, one can however conclude that the required distributions deviate substantially from the ISM size distribution (m=3.5, $a_{\rm min} \simeq 0.025$ and $a_{\rm max} \simeq 0.25\,\mu$m). Substantial grain growth/coagulation must have taken place to produce the required grain size distributions. The maximum grain size required to fit the 10 μm silicate feature (5 μm in our best fit model) depends, to a lesser extent, also on the strength of the underlying continuum at the long wavelength tail of this feature. Assuming the carbonaceous grains to be graphitic results in a slightly higher continuum contribution at these wavelengths, resulting in a smaller maximum size for the silicate dust by a

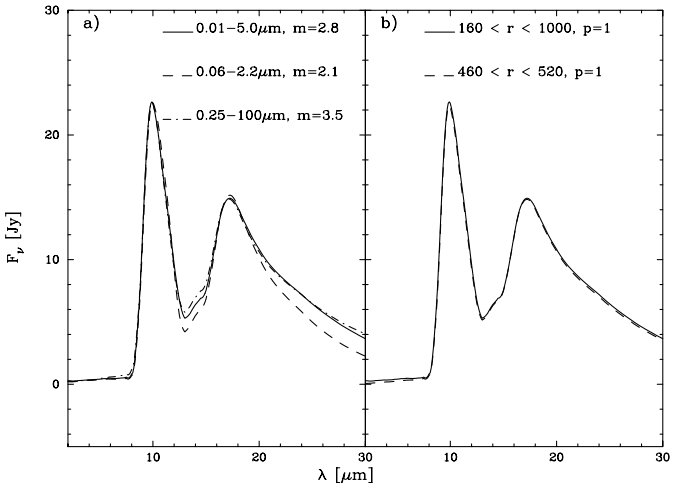

Fig. 5a and b. Degeneracies in the model fits. Panel **a** shows three model fits to the 10 μm silicate feature of AB Aur for different grain size distributions. Indicated in the figure are the minimum and maximum grain size and power m (see Eq. 2). Panel **b** shows the degeneracies in the dust density distribution. The density at the inner edge is $7.15{\cdot}10^{-19}$ (solid line) and $2.06 \cdot 10^{-19}$ gr cm^{-3} (dashed line) respectively for the two models. Indicated in the figure are the inner and outer radii (in stellar radii) between which the dust shells are confined and the power of the density distribution p (see Eq. 1). The solid lines in both panels represent the best model fit to the silicate component in AB Aur (see also Table 3).

factor of two, compared to the assumption of an amorphous carbonaceous dust component.

Between 14 and 20 μm the spectra are characterized by a strong rise in flux. This rise can be attributed to O-Si-O bending modes in the amorphous silicates around 18 μm. However, between 20 μm and the wavelengths where the cold dust starts to dominate the spectra, an additional solid-state emission component, apart from the silicate, is required to explain the observed fluxes. This broad emission complex is most clearly seen in HD 163296. Apart from the broad resonances in the near-IR, which may contribute to the observed flux in this region, iron oxide has a strong spectral feature between 21 and 25 μm, depending on grain shape (Begemann et al. 1995). Only by including non-spherical FeO grains a satisfactory model fit could be obtained. Because we calculated the optical properties of FeO entirely in the Rayleigh limit, no information about grain sizes could be obtained for this species (see also Sect. 2).

How well constrained are the results listed in Table 3 for the hot dust component? Apart from degeneracies in the model fits due to a lack of clear spectral signatures and the uncertainties in the grain size distribution, both discussed above, another degeneracy may be identified (Bouwman et al. 1999). As an example for this degeneracy, Fig. 5b shows two model fits to the silicate component in AB Aur, both having the same mass averaged temperature, but with different density distributions, resulting in identical spectra. This example is equally valid for the other dust species around AB Aur as well as around HD 163296. As discussed in the previous subsection, to explain the observed NIR fluxes the dust grains have to be heated to their destruction temperatures, which determines the inner radius of the dust distribution of the individual dust species. With the assumption that all dust species are well mixed and that, therefore, the only spatial separation between species is caused by differences in grain destruction temperatures, resulting in different inner radii, the density distributions listed in Table 3 are the most likely ones.

3.3. The cold dust component

Figs. 1 and 2 also show the ISO-LWS spectrum of AB Aur, the one star for which we also have LWS observations. For wavelengths exceeding the LWS wavelength range for AB Aur and for wavelengths exceeding the ISO-SWS wavelengths for HD 163296, we only have photometric points. This means that far less information about the chemical composition can be derived at these wavelengths than from the ISO-SWS spectra, also because the LWS spectrum does not show any discrete spectral signatures. To get around this problem we have taken the chemical composition of the hot dust component, derived from the SWS spectra, and used the same material to model the cold dust component. The main difference is the inclusion of water ice as component of the cold dust. We further assume that all iron is locked up in amorphous silicate grains and, as a minor constituent, in iron oxide. This is suggested by the temperature distribution of the metallic iron in the hot dust component which, having a minimum temperature of $\sim$ 700 K, suggests a presence of metallic iron only at the inner edge of the hot dust component. Also the sharp rise in flux levels between 40 and 60 μm points to the absence of metallic iron in the cold dust, as including this dust species would tend to flatten out the SED in this region, in contradiction with the observations. Evidence for crystalline H_2O ice was found in the Herbig star HD 142527 (Malfait et al. 1999), and is expected to be present in the outer parts of proto-planetary disks. The inclusion of H_2O ice significantly improves the quality of the fit in the 40–80 μm wavelength range. Only by adding H_2O ice as a dust constituent the correct slope could be reproduced as a result of the strong 60 μm feature of water ice. Tabel 3 lists the model parameters of the best fit to the cold dust component. The listed relative abundances are, due to confusion of the relative contribution of the individual dust species, uncertain by a factor of two.

In the current model a gap of $\sim$ 20 AU is required between the hot and the cold dust component in order to create the required bi-model temperature structure. We will come back to this point in the next section.

The spectral energy distribution at sub-mm to radio wavelengths is determined by the temperature and density distribution of the cold grains, as well as by their (average) grain size. (Sub)-mm and radio imaging constrain the location of these cold grains to distances less than several 100 AU. Using these constraints, a population of large ($\sim$ 1 and $\sim$ 0.1 mm for HD 163296 and AB Aur respectively) grains is required to reproduce the observed shape of the SED from sub-mm to radio wavelengths. Large grains ($>$ 1 mm) radiate as black bodies at mm wavelengths, and the Rayleigh-Jeans part of the SED of HD 163296 can naturaly be explained by such grains emitting at tempera-

tures > 20 K. The spectral shape of AB Aur at these long wavelengths is significantly steeper than that of a Rayleigh-Jeans tail (of a black body), hence smaller grains dominate the SED.

Our model fit gives a maximum grain size of ~ 0.1 mm, a factor of ten smaller compared to HD 163296. As stated above, these results are derived by constraining the dust distribution with the available image data. However, relating the predicted mass over temperature distribution to the exact spatial distribution imposed by the imaging depends on the correctness of the model assumptions, i.e. on whether the assumption that the medium is optically thin is correct. Shielding of direct stellar radiation by an optically thick dust distribution will modify the temperature-distance relation of the grains, and consequently will change the spatial distribution of the dust considerably compared to an optically thin model with the same mass over temperature distribution (see Sect. 6 for further discussion). The question therefore is: can one relate the current model directly to the image data? Adopting the same grain sizes as derived for the hot dust component, i.e. assuming a maximum grain size of a few micron, the cold dust of AB Aur can only be fitted with our optically thin model if the grains are about a factor of 10 further out than imposed by the image data. If considerable optical depth effects are present in the dust around AB Aur the dust could be moved inwards, having the same temperatures as in the optically thin model, thus complying with the observations without the need for large grains. However, in the case of HD 163296 we want to point out that it is not possible to fit the observed slope of the SED at mm wavelengths using our optically thin model and an identical size distribution as derived for the hot dust component. As optical depth effects primarily affect the location of the dust and not the slope of the far-IR spectrum, which in both an optically thin and thick medium is essentially transparent for locally emitted radiation, this result will also be valid for an optically thick model. Therefore, even if optical depth effects play a role in HD 163296, the grains needed to explain the sub-mm to radio wavelength part of the SED need to be of the same size (~ 1 mm) as predicted in our optically thin model.

3.4. PAHs and crystalline silicates

Fig. 6 shows the residue of the ISO-SWS spectra subtracted by the best fit dust continuum for AB Aur and HD 163296. Clearly visible are the PAH bands in AB Aur and the forsterite bands in HD 163296, where we have over-plotted the model fit to this component. A forsterite component has to be present in *both* the hot and in the cold dust component to reproduce all observed features. The presence of this cold crystalline material poses some interesting problems. While in the hot dust component the temperatures are sufficient to have thermal annealing at sufficiently short time scales compared to the dynamic time scales of these systems to produce crystalline silicates (e.g. Gail 1998), this is not the case for the cold dust component. This would suggest that either extensive mixing between the cold and the hot regime has taken place, or that crystallization at low temperatures can take place by means of a non-thermal annealing process of the amorphous silicates (Molster et al. 1999). Another interesting problem is the difference in grain size between the forsterite and the amorphous olivine (see Table 3) for our best model fit. The requirement that the forsterite in the cold dust component has to reproduce the emission feature at 33.6 μm limits the maximum grain size to ~ 5 μm. This is much smaller than the average size of the amorphous grains (~ 1 mm) in the cold component of HD 163296. Adopting similar large grain sizes for the crystalline silicates in the cold component would not produce any observational emission band at 33.6 μm due to the large grain size compared to the wavelength. This does *not* imply, however, that large crystalline grains can be excluded. Large (> 100 μm) crystalline grains effectively have the same spectroscopic behaviour as amorphous grains and are thus spectroscopically indistinguishable from amorphous grains. The above does however imply that there is no continuous grain size distribution from small (~ 0.1 μm) to large (~ 1 mm) grains for the forsterite. A bi-model grain size distribution remains a possibility, where the smaller grains (say up to 5 μm) could reproduce the flux between 40 and 100 μm and a population of large grains would be responsible for the (sub)millimetre fluxes.

The modelling of the PAH bands observed in AB Aur is beyond the scope of this paper. The 6.2 μm band caused by the C-C strech of the bonds in a benzene ring (Schutte et al. 1993) is at 6.25 μm in AB Aur, while in most other objects it is close to 6.22 μm. Furthermore, the absence of the 3.3 μm PAH feature suggests processing of the PAH molecules (Peeters et al. in prep).

4. Discussion

An important result of the presented study is that the circumstellar material around both AB Aur and HD 163296 is characterized by a bi-modal mass over temperature distribution. This dichotomy is presented in Fig. 7. The left panels show the distribution for AB Aur; the right panels that for HD 163296. Upper panels show the hot component; lower panels the cool component. The choice of the vertical axis unit ensures that the integral of each shaded region (representing different species) reflects the total mass per component. Note the large difference in scaling of the vertical axis for the hot, respectively cold dust. The inset panel shows the warmest dust in the cold component in the same scaling as the hot component.

The presented mass over temperature distribution reflects the dust properties responsible for the observed SED and holds irrespective of the assumed model geometry and/or associated optical depth. In our optically thin model, the dichotomy in the temperature distribution can only be explained if we assume a physical gap of ~ 20 AU between the hot and cold component. These two separate dust shells are really necessary, as even a bi-modal grain size distribution, consisting of small hot grains and larger cooler grains cannot solve this problem.

As discussed in Sect. 1, imaging shows a disk like structure around AB Aur and HD 163296. The bi-modal temperature distribution may therefore perhaps be naturally explained with the cold dust distributed in an optically thick disk and the hot dust

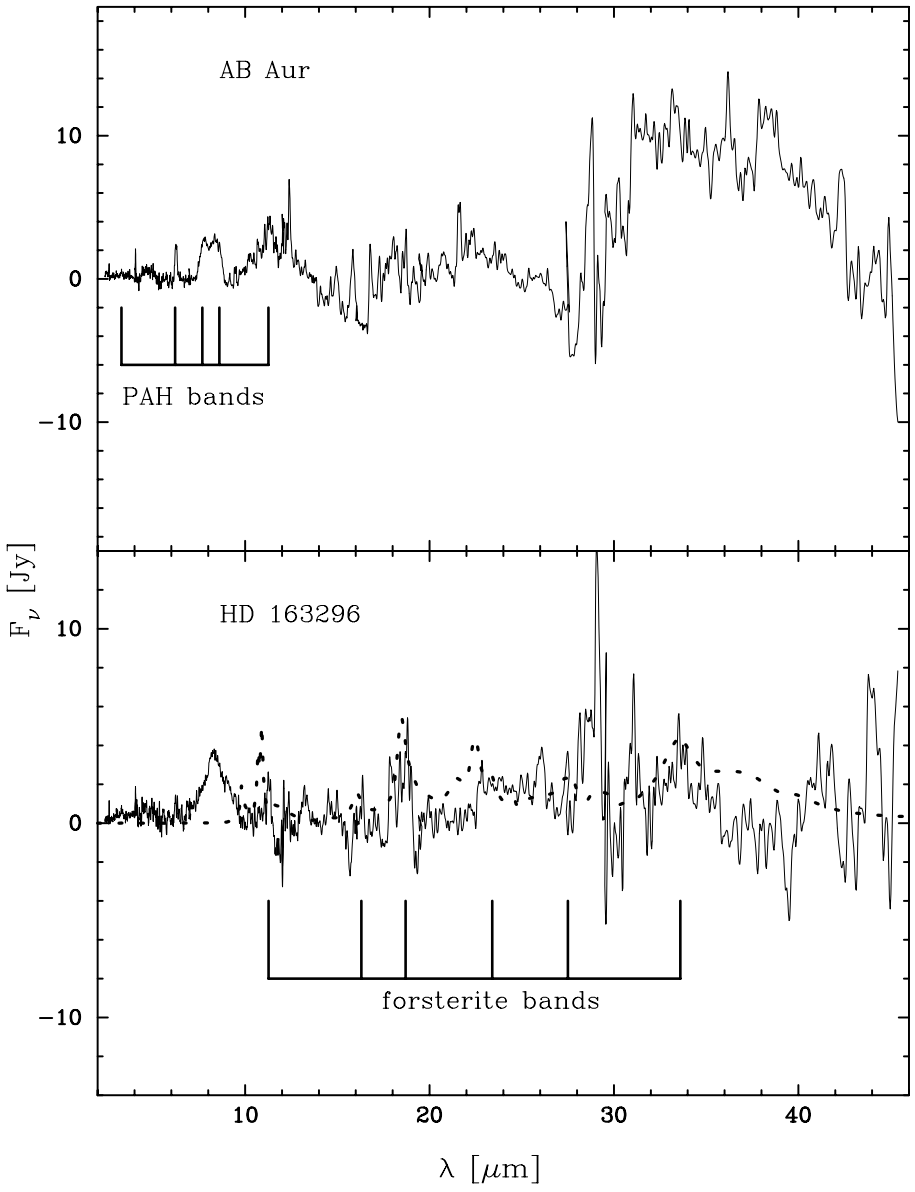

Fig. 6. Residual spectra of AB Aur (top) and HD 163296 ISO SWS spectra subtracted by the current best model fit. Indicated in top panel with the thick vertical lines are the positions of the main features attributed to polycyclic aromatic hydrocarbons (PAH) bands at 3.3, 6.2, 7.7 8.6 and 11.3 μm for AB Aur; and in the lower panel are indicated the main features of forsterite at 11.3, 16.3, 18.7, 23.4, 27.5 and 33.6 μm for HD 163296. The dotted line represent the best model fit for forsterite.

in an optically thin surface layer or extended atmosphere on top of this disk. In this model, a discontinuity in the spatial dust distribution may not be needed. Fig. 8 shows a schematic outline of such a disk geometry. The dense, optically thick inner regions of the disk shield material located somewhat farther out from direct illumination by stellar radiation. In a dust distribution which is optically thick both to locally and non-locally emitted radiation, the temperature as a function of radial distance will drop as T$\propto R^{-3/4}$. In an optically thin medium the temperature is expected to drop as T$\propto R^{-2/5}$ (assuming the dust opacity is proportional to λ^{-1}). This means that in the optically thick case, a given temperature is reached closer to the star. Fig. 8 also shows the schematic run of temperature for two radial paths through the proto-planetary disk: path A represents a beam for which the optical depth τ is less than unity, therefore T is relatively high; while path B represents a beam for which $\tau > 1$, therefore the temperature is relatively low. The difference in optical depth between the hot and cold component seems consistent with the difference in mass in both these components, i.e. the hot dust contains of the order of $\sim 10^4$–10^5 less mass than does the cold dust.

The above model could in principle reproduce the mass over temperature distribution of the cold dust closer to the star compared to our optically thin model and thus could bridge the gap between the hot and cold component, resulting in a more continuous dust distribution. Indeed, more detailed modeling of proto-planetary disks (e.g. Chiang & Goldreich 1997; Men'shchikov & Henning 1997) shows that the required bi-modal temperature distribution can occur in an optically thick disk.

Still, the possibility that a hot and cold dust component are physically separated can not be excluded. The presence of a large mass, such as a proto-planet, clearing a part of the disk could be an explanation for such a distribution. This is also suggested by a previous study of the shape of the energy distribution

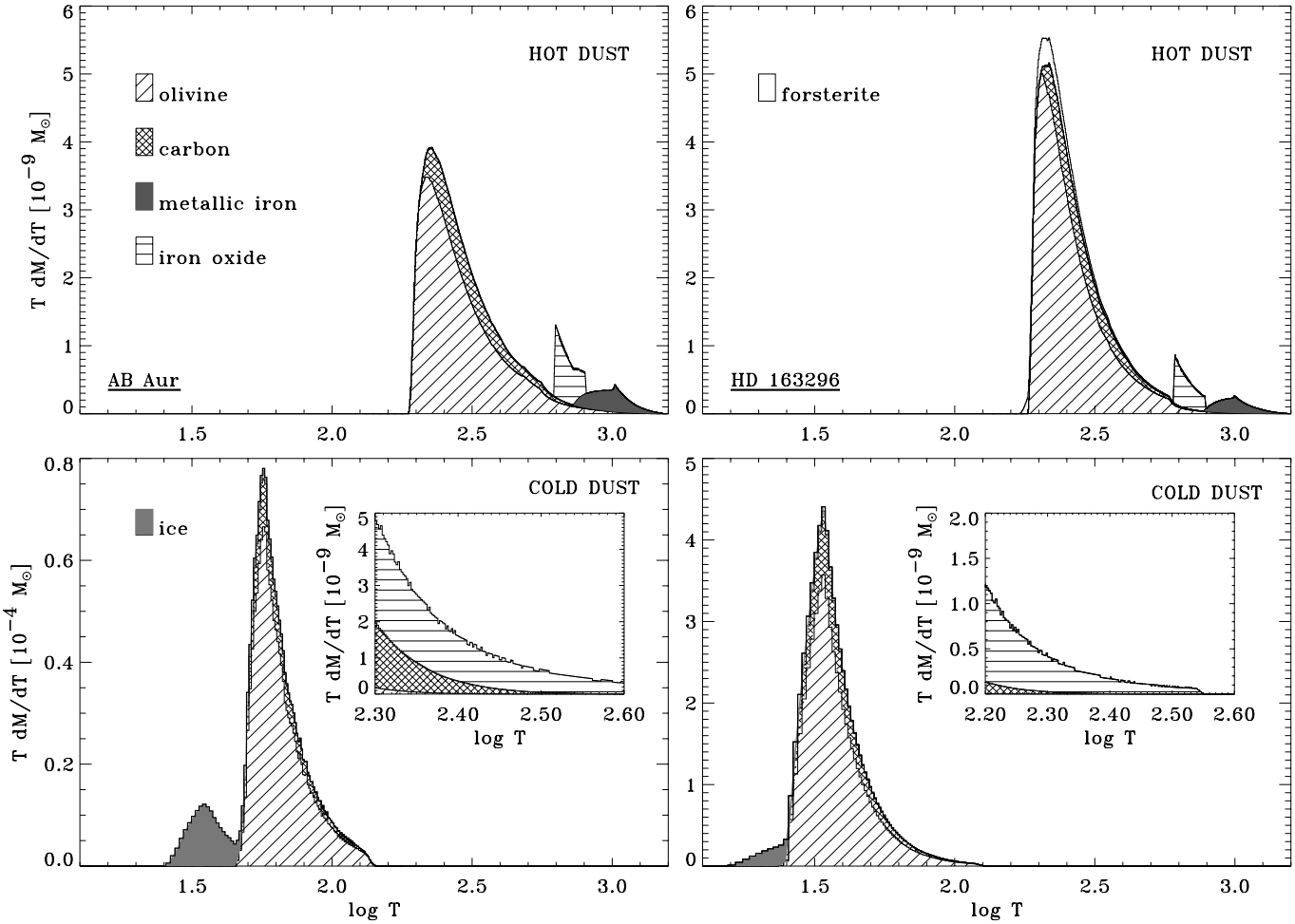

Fig. 7. Cumulative dust mass over temperature distribution. The left panels show the distribution for AB Aur, and the right panels that for HD 163296. The top panels show the hot dust component and the bottom panels the cold dust distribution. Indicated in the figures are the relative contributions of the individual dust species. The inset figures in the bottom panels show the warmest dust of the cold dust component, being dominated by the iron oxide grains. Note that the scale of the y-axis differs for the bottom panels, which is in units of $10^{-4}\mathrm{M}_{\odot}$ for both panels.

of a sample of HEABE stars (Malfait et al. 1998a). Evidence for larger bodies around Herbig Ae stars is suggested by observations of infalling circumstellar material. The observed velocities of the infalling gas seem consistent with infalling and evaporating larger bodies (Grady et al. 1999).

The chemical composition of the dust closest to the central star is determined by the dust destruction temperatures of the individual dust species. As can be seen from Fig. 7, the mass at the highest temperatures is dominated by metallic iron. At lower temperatures the iron is not in the form of metallic iron but is incorporated in iron oxide and silicates. This is suggestive of chemical processing of the dust. The dust, being slowly accreted, is heated up thereby transforming iron oxide to metallic iron and releasing the iron by solid state reduction from the olivine. Several models for the chemical evolution of protoplanetary disks predict the presence of trolite (FeS) (e.g. Gail 1998; Pollack et al. 1994). This component is also found in meteorites and interplanetary dust particles (IDPs). However, using the optical constants measured by Henning & Stognienko (1996), which show a clear spectral signatures between 30 and 40 μm, no evidence could be found for the presence of this species.

The requirement of having dust grains at temperatures up to their destruction or condensation temperatures poses an interesting problem for the silicates. Silicate grains with a temperature in excess of $\sim$ 800 K, (much lower than the condensation temperature), can crystallize at time scales shorter than the age of the Herbig Ae stars (Gail 1998). The relatively small fraction of forsterite compared to that of amorphous olivine in HD 163296, and the complete absence of crystalline silicates in AB Aur seems in contradiction with these crystallization time scales.

A solution to this apparent problem is that we are not looking at a static mass distribution, but have a situation where the hot dust component is removed (by infall) and replenished with unprocessed material. The difference in spectral signature between AB Aur, where no crystalline silicates are detected and HD 163296 where a mass fraction of $\sim$ 0.1 in the hot dust component is in crystalline form, could be explained in terms

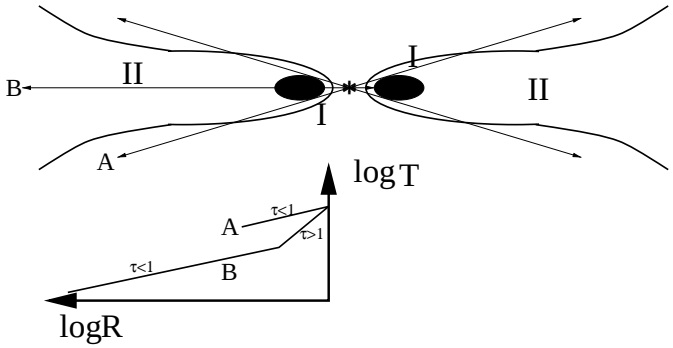

Fig. 8. Schematic representation of a proto-planetary disk. The dark area represent the part of the disk where optical depths in excess of one are reached. Area I is optically thin for all paths emanating from the central star and can be directly illuminated. Area II is shielded from direct illumination by the inner part of the disk. The inset figure gives a schematic temperature profile for two beams one through the disk along path B and missing the disk along path A.

of different rates of removal of the high temperature silicate grains.

The amount of forsterite that could be added to the hot dust component of AB Aur without causing a spectral signature is $\sim 10^{-11}$ $M_\odot$. To comply with observations, this amount is $\sim 10^{-10}$ $M_\odot$ for HD 163296. The total mass of silicate grains with a temperature above the crystallisation temperature is $\sim 10^{-10}$ $M_\odot$ for both AB Aur and HD 163296. From a comparison of these masses with observed accretion rates of 1.1×10^{-10} and $< 9.1 \times 10^{-11}$ $M_\odot yr^{-1}$ (assuming a dust to gass ratio of 0.01) for AB Aur and HD 163296 respectively (Skinner et al. 1993), one can conclude that it is possible to accrete the hot amorphous silicate grains at a short enough time scale before they give a significant spectral signature.

The presence of crystalline silicates in the cold dust around HD 163296 could be explained by vertical mixing in a disk between the hot, optically thin surface layer and the optically thick inner part, though non-thermal annealing of amorphous silicates is also a possibility (Molster et al. 1999).

5. Summary

1. We have modelled the energy distribution of AB Aur and HD 163296 using an optically thin dust model, and have derived the chemical composition and size distribution of the dust components contributing to the spectrum.
2. The SED of the Herbig Ae stars AB Aur and HD 163296 is characterized by a bi-modal mass over temperature distribution. A low mass ($\sim 10^{-9}$ $M_\odot$) dust component with temperatures of ~ 1000 K and a cold component (~ 100 K) which contains most of the mass ($\sim 10^{-5}$ to 10^{-4} $M_\odot$) is required to fit the SED.
3. The onset of the near-IR emission at 2 μm can be explained with emission from metallic iron grains.
4. In both stars substantial grain growth, compared to interstellar dust, has taken place, resulting in grain sizes up to ~ 0.1 mm around AB Aur and up to ~ 1 mm around HD 163296.
5. The grain growth around HD 163296 has been more substantial than around AB Aur. Together with the presence of crystalline silicates in the former star, this suggests that HD 163296 is a more evolved system than AB Aur.

Acknowledgements. The authors would like to acknowledge the financial support from NWO *Pionier* grant 600-78-333 and from NWO/NFRA grant 781-76-015. AdK also gratefully acknowledges support from NWO Spinoza grant 08-0 to E.P.J. van den Heuvel.

References

Begemann B., Henning Th., Mutschke H., Dorschner J., 1995, P&SS 43, 1257
Biermann P., Harwit M., 1980, ApJ 241, L105
Böhm T., Catala C., 1993, A&AS 101, 629
Böhm T., Catala C., 1995, A&A 301, 155
Bohren C.F., Huffman D.R., 1983, Absorption and Scattering of Light by Small Particles, John Wily & Sons inc
Bouwman J., de Koter A., van den Ancker M.E., Waters L.B.F.M., 1999, ASP Conf. Ser., in Press
Bradley J.P., Humecki H.J., Germani M.S., 1992, ApJ 394, 643
Chiang E.I., Goldreich P., 1997, ApJ 490, 368
Cohen M., 1980, MNRAS, 191, 499
Corcoran M., Ray T.P., 1997, A&A 321, 189
Crovisier J., Leech K., Bockelee-Morvan D., et al., 1997, Sci 275, 1904
Dominik C., Gail H.-P, Sedlmayer E., 1989, A&A 223, 227
Dorschner J., Begemann B., Henning Th., Jaeger C. Mutschke H., 1995, A&A 300, 500
Duschl W.J., Gail H.-P., Tscharnuter W.M., 1996, A&A 312, 624
ESA, 1997, The Hipparcos Catalogue, ESA SP-1200
Finocchi F., Gail H.-P., Duschl W.J., 1997, A&A 325, 1264
Fitzpatrick E.L., 1997, IAUS 187
Fitzpatrick E.L., Spitzer L. Jr. 1997, ApJ 475, 623
Gail H.-P., 1998, A&A 332, 1099
Gail H.-P., Sedlmayr E., 1999, A&A 347, 594
Gaposchkin C.H.P., Gaposchkin S., Menzel D.H., 1952, AnHar 118
Grady C.A., Pérez M.R., Bjorkman K.S., Massa D., 1999, ApJ 511, 925
Halbedel E.M., 1996, PASP 108, 833
Henning Th., 1997, In: van Dishoeck E.F. (ed.) Molecules in Astrophysics: Probes and Processes. p. 343
Henning Th., Stognienko R., 1996, A&A 311, 291
Henning T., Begemann B., Mutschke H., Dorschner J., 1995, A&AS 112, 143
Henning Th., Burkert A., Launhardt R., Leinert Ch., Stecklum B., 1998, A&A 336, 565
Hillenbrand L.A., Strom S.E., Vrba F.J., Keene J., 1992, ApJ 397, 613
Houk N., Smith-Moore A., 1988, Michigan Spectral Survey Vol. 4, Univ. Michigan Press
Jones A.P., 1990, MNRAS 245, 331
Kessler M.F., Steinz J.A., Anderegg M.E., et al., 1996, A&A 315, 27
Laor A., Draine B.T., 1993, ApJ 402, 441
Malfait K., Bogaert E., Waelkens C., 1998a, A&A 331, 211
Malfait K., Waelkens C., Waters L.B.F.M., et al., 1998b, A&A 332
Malfait K., Waelkens C., Bouwman J., de Koter A., Waters L.B.F.M., 1999, A&A 345, 181
Mannings V. Sargent A.I., 1997, ApJ 490, 792
Mannings V., Koerner D.W., Sargent A.I., 1997, Nat 388, 555
Marsh K.A., Van Cleve J.E., Mahoney M.J., Hayward T.L., Houck J.R., 1995, ApJ 451, 777

Mathis J.S., Rumpl W., Nordsieck K.H., 1977, ApJ 217, 425
Meeus G., Waelkens C., Malfait K., 1998, A&A 329, 131
Men'shchikov A.B., Henning T., 1997, A&A 318, 879
Millan-Gabet R., Schloerb F.P., Traub W.A., et al., 1999, ApJ 513, L131
Molster F.J., Yamamura I., Waters L.B.F.M., et al., 1999, Natur 401, 563
Natta A., Prusti T., Krugel E., 1993, A&A 275, 527
O'Donnell J.E., Mathis J.S., 1997, ApJ 479, 806
Pollack J.B., Hollenbach D., Beckwith S., et al., 1994, ApJ 421, 615
Preibisch Th., Ossenkopf V., Yorke H.W., Henning Th., 1993, A&A 279, 577
Schulze H., Kissel J., Jessberger E.K., 1997, In: Pendleton Y.J., Tielens A.G.G.M. (eds). From Stardust to Planetesimals. ASP Conf. Ser. 122, p. 397
Schutte W.A., Tielens A.G.G.M., Allamandola L.J., 1993, ApJ 415, 397
Scott A., Duley W.W., 1996, ApJS 105
Servoin J.L., Piriou B., 1973, Phys. Stat. Sol. (b) 55
Sitko M.L., 1981, ApJ 247, 1024
Skinner S.L., Brown A., Stewart R.T., 1993, ApJS 87, 217
van den Ancker M.E., Thé P.S., Tjin A Djie H.R.E., et al., 1997, A&A 324, L33
van den Ancker M.E., de Winter D., Tjin A Djie H.R.E., 1998, A&A 330, 145
van den Ancker M.E., Bouwman J., Wesselius P.R., Waters L.B.F.M., van Dishoeck E.F., 2000, A&A 357, 325
Warren S.G., 1984, Applied Optics 23, 1206
Waters L.B.F.M., Waelkens C., 1998, ARA&A 36, 233